Full length article

Stress measurements by multi-reflection grazing-incidence X-ray diffraction method (MGIXD) using different radiation wavelengths and different incident angles

Marianna Marciszko [a, *], Andrzej Baczmański [b], Chedly Braham [c], Mirosław Wróbel [d], Sebastian Wroński [b], Grzegorz Cios [a]

[a] AGH University of Science and Technology, ACMIN, al. Mickiewicza 30, 30-059, Kraków, Poland
[b] AGH University of Science and Technology, WFiIS, al. Mickiewicza 30, 30-059, Kraków, Poland
[c] Arts et Métiers-ParisTech, PIMM, CNRS UMR 8006, 151 Bd de l'Hôpital, 75013, Paris, France
[d] AGH University of Science and Technology, WIMIP, al. Mickiewicza 30, 30-059, Kraków, Poland

A B S T R A C T

The presented study introduces the development of the multi-reflection grazing-incidence X-ray diffraction method (MGIXD) for residual stress determination. The proposed new methodology is aimed at obtaining more reliable experimental data and increasing the depth of non-destructive stress determination below the sample surface. To verify proposed method measurements were performed on a classical X-ray diffractometer (Cu Kα radiation) and using synchrotron radiation (three different wavelengths: λ = 1.2527 Å, λ = 1.5419 Å and λ = 1.7512 Å). The Al2017 alloy subjected to three different surface treatments was investigated in this study. The obtained results showed that the proposed development of MGIXD method, in which not only different incident angles but also different wavelengths of X-ray are used, can be successfully applied for residual stress determination, especially when stress gradients are present in the sample.

Keywords:
Residual stress
X-ray diffraction
Synchrotron radiation
Grazing

1. Introduction

Residual stress can result from temperature or deformation gradients which are present in almost every step of material processing. They can occur as a consequence of various technological treatments and manufacturing processes but they can also arise in the component during its service life. Therefore, both the magnitude and the spatial distribution of residual stresses have to be analysed in detail in order to understand the behaviour of material subjected either to heat treatment or plastic deformation, especially in the surface region. The great need for precise and non-destructive determination of stress has resulted in the development of new measuring methods. Among them X-ray diffraction techniques are common methods for stress determination in the surface layers of the materials. In fact, in diffraction stress investigation the interatomic lattice spacing and thus elastic strain are measured directly. However, stress and strain are tensor quantities which are related to one another by the elastic stiffness tensor. One should be aware of the significance of the X-rays absorption and therefore the information depth on stress determination. This effect is of particular concern when the gradient of stress is present in the sample.

The mean lattice strain $<\varepsilon(\phi,\psi,\bar{z})>$ at information depth $\bar{z}$, calculated over reflecting grains can be related with the mean first order stress according to the following equation [1,2]:

* Corresponding author.
E-mail addresses: marianna.marciszko@fis.agh.edu.pl (M. Marciszko), andrzej.baczmanski@fis.agh.edu.pl (A. Baczmański), chedly.braham@paris.ensam.fr (C. Braham), mwrobel@agh.edu.pl (M. Wróbel), sebastian.wronski@fis.agh.edu.pl (S. Wroński), grzegorz.cios@agh.edu.pl (G. Cios).

$$<\varepsilon(\phi,\psi,\bar{z})>_{\{hkl\}} = \frac{<d(\phi,\psi,\bar{z})>_{\{hkl\}} - d^0_{\{hkl\}}}{d^0_{\{hkl\}}} = \frac{\int_0^t <d(\phi,\psi,\bar{z})>_{\{hkl\}} e^{-z/\tau} dz}{d^0_{\{hkl\}} \int_0^t e^{-z/\tau} dz} \quad (1)$$

$$= F_{ij}(hkl,\phi,\psi)\sigma^I_{ij}(\bar{z})$$

where: $\sigma^I_{ij}(\bar{z}) = \int_0^t \sigma^I_{ij}(z)e^{-z/\tau}dz / \int_0^t e^{-z/\tau}dz$ and $\langle d(\phi,\psi)\rangle_{hkl}$ are interplanar spacings (determined from diffraction peak positions), $F_{ij}(hkl,\phi,\psi)$ are the X-ray Stress Factors (XSF), ϕ is the azimuthal angle between measuring direction and direction along which the principal component σ is defined, ψ polar angle describes the inclination of the diffraction vector with respect to the sample normal (for strict definition see for example [1,3,4]), t is the sample thickness, τ is the 'penetration depth' defined as the distance from the surface of bulk material ($t \to \infty$), for which $(1-1/e) = 0.63$ part of total intensity of the incident beam is absorbed (τ depends on absorption factor and geometry of measurement).

The above average corresponds to so-called 'information' or 'effective' depth $\bar{z}$, which can be understood as the mean value of z-depth weighted by an attenuation factor [2]:

$$\bar{z} = \frac{\int_0^t z\exp(-z/\tau)dz}{\int_0^t \exp(-z/\tau)dz} = \begin{cases} \tau - \dfrac{\tau\exp(-t)/\tau}{1-\exp(-t)/\tau} & \text{for limited } t \\ \tau & \text{for } t\to\infty \end{cases} \quad (2)$$

In order to reveal the real depth profile of stress $\sigma^I_{ij}(z)$, it is necessary to perform inverse Laplace transformation for the data gained experimentally $\sigma^I_{ij}(\bar{z}=\tau)$ [5–7].

The great need for precise stress determination has involved the introduction of new measuring methods and devices into the experimental world. One of them is multi-reflection grazing-incidence X-ray diffraction (MGIXD) geometry [8], also called multiple {hkl} grazing incidence [9]. This method is characterised by a small and constant incidence angle α and by different orientations of the scattering vector $\mathbf{\Delta K}$ (variable $2\theta_{\{hkl\}}$ angle for a constant wavelength; see Fig. 1) given by the equation:

$$\psi_{\{hkl\}} = \theta_{\{hkl\}} - \alpha \quad (3)$$

where: $2\theta_{\{hkl\}}$ are the diffraction angles corresponding to those reflections hkl for which diffraction peaks are measured [8,10,11].

In this geometry the diffraction plane (defined by incident and diffracted beam) is always perpendicular to the sample surface and the penetration depth is given by Ref. [10]:

$$\tau = \left(\frac{\mu}{\sin\alpha} + \frac{\mu}{\sin(2\theta_{\{hkl\}} - \alpha)}\right)^{-1} \quad (4)$$

where: μ is the linear absorption coefficient of X-rays in the studied material.

Stress can be determined from the interplanar spacings measured in direction of the scattering vector; in this case it means for different $\psi_{\{hkl\}}$ and consequently various $\theta_{\{hkl\}}$ angles but for a constant α angle (Fig. 1). It is convenient to use for the MGIXD method, instead of $<d(\phi,\psi,\bar{z})>_{\{hkl\}}$, the so called equivalent lattice parameters $<a(\phi,\psi,\bar{z})>_{\{hkl\}}$ and to express them with the macrostresses $\sigma^I_{ij}(\bar{z})$ and strain free lattice constant a_0 [3,4,8,10,11]:

$$<a(\phi,\psi,\bar{z})>_{\{hkl\}} = [F_{ij}(hkl,\phi,\psi)\sigma^I_{ij}(\bar{z})]a_0 + a_0 \quad (5)$$

where, for cubic crystal structure: $<a(\phi,\psi,\bar{z})>_{\{hkl\}} = <d(\phi,\psi,\bar{z})>_{\{hkl\}}\sqrt{h^2+k^2+l^2}$, the ψ depends on the diffraction angle for the given reflection hkl (Eq. (3)), while the ϕ angles should be chosen taking into account symmetry of the sample.

In the case of the MGIXD method, the measurements of interplanar spacings $\langle d(\phi,\psi,\tau)\rangle_{\{hkl\}}$ are performed in the near surface volume, limited by radiation absorption. Using Eq. (5) and assuming $\sigma^I_{33}(\tau) = 0$, the other parameters of the stress tensor and a_0 parameter can be determined from the least square fitting procedure. On the other hand, if the value a_0 is known, the full stress tensor can be found for given τ or $\bar{z}$. This provides a possibility to measure a stress gradient as well as the in-depth dependence of a_0. The great advantage of this method is that for a given α angle, the penetration depth is constant and therefore it is possible to perform

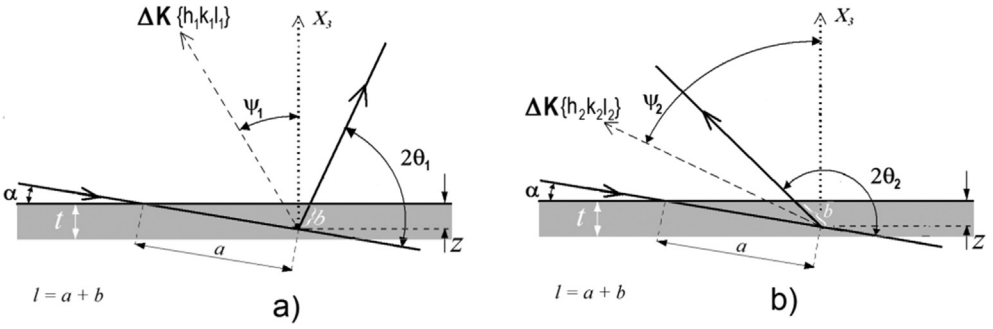

Fig. 1. Geometry of the MGIXD-sin$^2\psi$ method. Two different orientations of the scattering vector with respect to the sample (different $\psi_{\{hkl\}}$ and $2\theta_{\{hkl\}}$ angles) for fixed incidence angle α are shown in figures (a) and (b).

non-destructive stress measurements for different layers under the surface of the sample. More detailed information about the presented method has been widely described for example in the following references: [3,4,8,10–12].

In this study, attention will be paid to the possibility of measuring stress evolution vs. depth below the sample surface with the methodology of data interpretation obtained not only for different incident angles but also using simultaneously different wavelengths (the 'multi-reflection' and also 'multi-wavelength' method). The advantage of this approach is that more experimental data are available for calculating the stresses.

2. Experimental

The MGIXD measurements were performed for mechanically treated surfaces of Al2017 alloy using firstly a PANalytical – X'Pert MRD X-ray diffractometer. The results obtained with classical X-ray diffraction were verified by synchrotron radiation in order to test the MGIXD method and to precisely designate the variation of stress in the function of depth. Measurements were performed at the G3 beamline at the DORIS III (HASYLAB) storage ring. MGIXD geometry was used to measure stress at different depths below the surface.

2.1. Sample preparation and characterisation

In this study, the Al2017 alloy exhibiting low crystal anisotropy was investigated. The composition of this material is given in Table 1, while the single crystal elastic constants and Zener anisotropy factor are collated in Table 2 [13]. Three different samples were prepared by using three different kinds of mechanical surface treatment:

a) grinding (the speed of rotation of the grinding wheel was 2000 rpm, while the work speed was 9 m/min.; several passes were carried out and in each pass a layer of 20 μm was removed);
b) polishing type I (two-directional manual polishing with 5 steps using emery papers: 800, 1200, 2000, 2500, 4000 grit; next, polishing paste was used for final treatment);
c) polishing type II (two-directional manual polishing with 1 step using emery paper 2000 grit).

The surface roughness Ra parameters for all the mechanically treated samples are presented in Table 3.

2.2. Laboratory classical monochromatic diffractometer

At first, measurements were performed using the MGIXD method on a classical diffractometer (Cu Kα radiation) in parallel beam configuration with a Göbel mirror (incident beam optics) and soller collimator (diffracted beam optics). Additionally, the orientation distribution functions (ODFs, see Ref. [14]) characterising crystallographic texture were determined for all the mechanically treated samples using Cu radiation in the reflection geometry. The penetration depth in the texture measurement was always larger than in the case of stress determination (MGIXD) and the gradients of texture were not considered in this study. It was found that the initial texture of the Al2017 material was approximately random. Polishing modifies the size of the crystallites but does not significantly change the texture, which remains almost isotropic after both types of polishing. The grinding process was the only one which changed the texture significantly. The ODF for the ground sample is presented in Fig. 2.

Table 2
Single crystal elastic constants and Zener anisotropy factor for aluminium [13].

Material	Single crystal elastic constants (GPa)			Zener factor
	C_{11}	C_{12}	C_{44}	
Al	106.8	60.4	28.3	1.22

Table 3
Values of surface roughness parameter (Ra) for investigated sample.

Surface treatment	Ra (μm)
Al2017	
Polishing type I	0.13
Polishing type II	0.27
Grinding	1.18

2.3. Synchrotron multiwavelength measurements

The results obtained with classical X-ray diffraction for the polished sample (type II) showed a high depth-dependent stress gradient and therefore they were verified using synchrotron radiation. The experiment was performed at the DORIS III (HASYLAB) storage ring, on beamline G3 spectrometer, equipped with a soller collimator (equatorial divergence 0.15°) and scintillation detector. A double-crystal germanium monochromator was used. The beam dimension at the monochromator was about 5 mm per 10 mm. All the monochromator movements were driven by stepper motors. A tilted gold mirror was used for suppression of the higher harmonics of the synchrotron radiation waves. The penetration depth during this experiment was changed by proper selection of the incident angle and wavelength. Three different wavelengths ($\lambda = 1.2527$ Å, $\lambda = 1.5419$ Å and $\lambda = 1.7512$ Å) were chosen and the corresponding incidence angles (α) for given penetration depths (τ) were calculated. The sets of incident angles and wavelengths corresponding to the assumed depths are presented in Table 4. The important question verifying the proposed methodology is: do we determine equal stresses for the combination of wavelengths and incident angles corresponding to the same penetration depth?

3. Results and discussion

3.1. Stress profile determined using laboratory diffractometer

The diffraction peak profiles obtained for different orientations of the scattering vector, as described by azimuthal angle ϕ and polar angle ψ, were successfully fitted by two pseudo-Voigt functions corresponding to $K_{\alpha 1}$ and $K_{\alpha 2}$ lines. Then, the $\langle a(\phi,\psi)\rangle_{\{hkl\}}$ lattice parameters were determined from the Bragg's law and using crystallographic relation between lattice parameter and interplanar

Table 1
Composition of the Al2017 alloy (wt%).

Material	Components								
Al 2017	Al bal.	Si 0.5	Fe 0.7	Cu 4.0	Mn 0.65	Mg 0.6	Cr 0.1	Zn 0.25	Ti 0.15

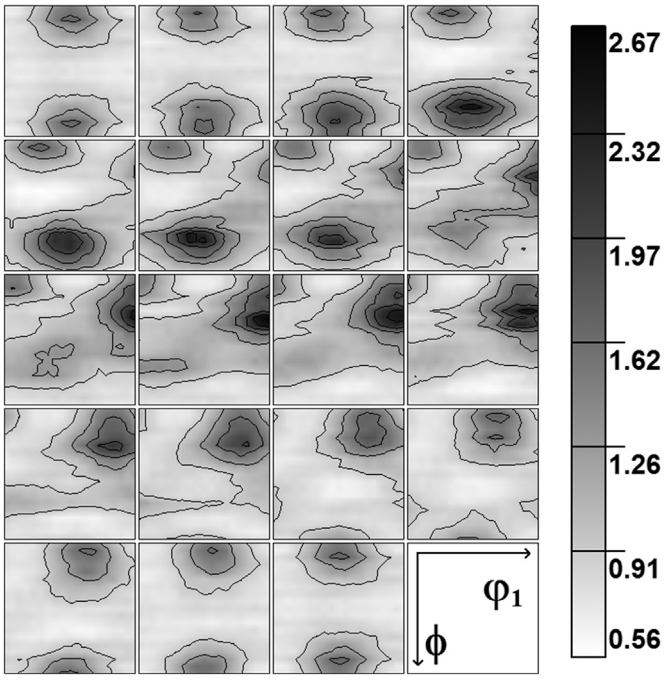

Fig. 2. Orientation distribution functions (ODF) determined using Cu Kα radiation for the ground Al2017 sample. The sections through Euler space [14] with the step of 5° are presented along the ϕ_2 axis: $0° \leq \phi_1, \Phi, \varphi_2 \leq 90°$.

spacing (see Eq. (5)). Fig. 3 shows examples of $\langle a(\phi,\psi)\rangle_{\{hkl\}}$ vs. $sin^2\psi$ plots measured for the polished (type II) and ground surfaces of the Al2017 alloy. The $\langle a(\phi,\psi)\rangle_{\{hkl\}}$ vs. $sin^2\psi$ plots were fitted using the procedure based on Eq. (5), with the XSF calculated by Eshelby-Kröner method [15] from the single crystal elastic constants given in Table 2. The influence of texture (cf. Fig. 2) on the XSF values was taken into account, but it was verified that this effect is not significant because of the low elastic anisotropy of the aluminium crystals. As shown in Fig. 3, in the ground sample a significant difference of the plot slopes was found for the two azimuth angles $\phi = 0°$ and 90°, contrary to the polished sample for which the slopes are almost equal.

The depth-dependent stress and a_0 lattice parameter profiles as a function of penetration depth (τ) were determined for different incident angles (α) for all the studied Al2017 samples. In Fig. 4, the obtained results were compared with measurements performed for the reference stress free Al powder. As was expected for the reference sample (Al powder), the stress was equal to zero (within the range of experimental uncertainty). In the ground sample, a tensile stress was generated due to the temperature gradient which is present during surface processing. The stress along direction of grinding (σ^I_{11}) is higher than in the transverse direction (σ^I_{22}). On the other hand, compressive stress $\sigma^I_{11} \approx \sigma^I_{22}$ was found in the polished samples. No significant depth-dependent evolution of stress was found for the samples after polishing type I or grinding, but a stress gradient occurred after polishing type II. No significant depth-dependent evolution of a_0 lattice parameter was observed for all the measured samples.

Table 4
Wavelengths λ, incident angles α and corresponding penetration depths used in synchrotron experiment.

λ = 1.2527 Å		λ = 1.5419 Å		λ = 1.7512 Å	
α (°)	τ (μm)	α (°)	τ (μm)	α (°)	τ (μm)
1.6	3.74	3	3.7	3	2.57
2.6	5.94	5	5.91	4.4	3.66
4.9	10.64	10	10.68	7.6	5.93
8.7	17.42	15	14.49	16	10.71
15	26.28	20	17.46		
20	31.42				

3.2. Stress profile using synchrotron radiation with different wavelengths

As it was mentioned earlier, for the sample having a significant gradient of stress (polishing type II), further investigation was performed using synchrotron radiation. Three different wavelengths (λ = 1.2527 Å, λ = 1.5419 Å and λ = 1.7512 Å) were used and the MGIXD method was applied, thereby extending the penetration depth (τ) for which the stress was determined. In order to check the agreement of the depth-dependent profiles obtained for different absorption of synchrotron radiation (depending on energy), the stress and a_0 parameter as the functions of penetration depth (τ) were determined for each wavelength, independently. The positions of the peaks were found by pseudo-Voigt function fitting or calculating the centre of gravity and next the fitting procedure, based on Eq. (5) with Eshelby-Kröner XSF, was applied to calculate the values of the stress $\sigma^I_{11} = \sigma^I_{22}$ (this assumption was previously confirmed by X-ray measurements) and a_0 parameter. When peaks were fitted by pseudo-Voigt function (Fig. 5a), a very good agreement was achieved between the data obtained using synchrotron radiation (for three different wavelengths) and classical diffractometer. If the peak positions are calculated as the centre of gravity (Fig. 5b), the agreement was not as good as in the case of pseudo-Voigt fitting but the stress was still equal, in the margin of uncertainty, for different wavelengths and classical diffractometer. Both methods (pseudo-Voigt and centre of gravity) gave very similar results.

It can be concluded that equal stress was determined for the combinations of wavelengths and incident angles corresponding to the same penetration depths. Therefore, our hypothesis that the measured mean interplanar spacings are weighted by absorption dependent factor (cf. Eq. (1)) was positively verified and the MGIXD method can be used to determine stress profile under sample surface. The agreement between stresses measured with different wavelengths of X-rays opened up the opportunity for MGIXD method development. The idea was to collect $\langle a(\phi,\psi)\rangle_{\{hkl\}}$ values corresponding to the same penetration depth τ on the same $sin^2\psi$ plot. Hence, $\langle a(\phi,\psi)\rangle_{\{hkl\}}$ vs. $sin^2\psi$ curves (containing information obtained using different wavelengths) were presented on separate plots corresponding to the chosen penetration depths (Fig. 6). Subsequently, the MGIXD method based on Eq. (5) was simultaneously applied for all $\langle a(\phi,\psi)\rangle_{\{hkl\}}$ values measured at the same penetration depth, as determined by a combination of chosen wavelength and incident angle. The XSF calculated by Eshelby-Kröner method were used for stress determination. As can be seen in Fig. 6, the experimental points are close to the fitted lines and a systematic decrease of the negative slope of the $\langle a(\phi,\psi)\rangle_{\{hkl\}}$ vs. $sin^2\psi$ plot (representing compressive stress) with penetration depth can be seen for both the experimental and fitted results. The stress depth-dependent profile obtained with the developed method is presented in Fig. 7a. The advantage of this approach is that each point on the depth-dependent profile was obtained not only with different reflections *hkl* corresponding to different incident angles (multi-reflection), but also with different wavelengths (multi-wavelengths). In consequence, the results are statistically more reliable because they are obtained as an average over a great number of polycrystalline grains.

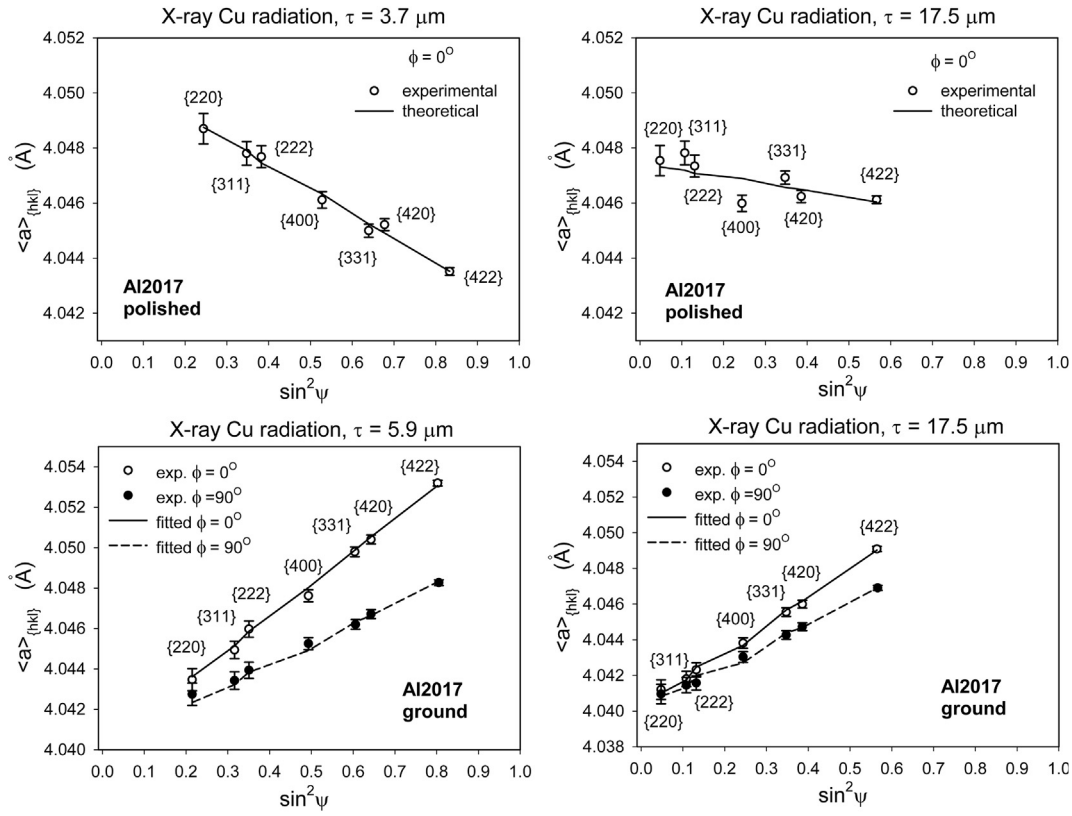

Fig. 3. An example of the ⟨a(ϕ,ψ)⟩{hkl} vs. $\sin^2\psi$ plots for different penetration depths in the polished-type II (a) and ground (b) samples. A significant difference between the plots for $\phi = 00$ and $\phi = 900$ is observed in the case of the ground sample.

Finally, the stress profile in the function of real depth z was determined using inverse Laplace transformation (for details, see Refs. [5,6]). To do this, the experimentally determined dependence of stress σ^I_{11} vs. penetration depth τ was approximated by second and third order polynomials. Then, the stress evolution in function of the real depth $\sigma^I_{11}(z)$ was determined assuming a bulk material for which the experimental values are defined as the averages of the $\sigma^I_{11}(z)$ function calculated from the surface to the infinite depth (i.e. $t \rightarrow \infty$ in Eqs. (1) and (2)). In Fig. 7b, the $\sigma^I_{11}(z)$ functions determined from both polynomials are presented with the calculated upper and lower uncertainty bounds. Almost identical solutions were obtained for both orders of polynomials.

3.3. *Analysis of the diffraction peak asymmetry caused by the stress gradient*

In the context of the stress profile $\sigma^I_{11}(z)$ presented in Fig. 7b, two important issues should be considered. Firstly, the function $\sigma^I_{11}(z)$ must be truncated at some depth z. Due to exponential attenuation of the X-ray beam, the influence of the stresses on the measured mean values $\sigma^I_{11}(\tau)$ decreases with increasing depth. Although, the stresses at a great depth can be determined from the inverse Laplace transform, their relative contribution on the experimental values becomes negligible due to relatively low intensity of the reflected X-ray beam. Therefore, the z-threshold over which the $\sigma^I_{11}(z)$ function looses its physical meaning should be estimated.

Secondly, it should be considered whether the determined stress gradient explains the asymmetry of the diffraction peak measured using synchrotron radiation. It should be noted that in the case of synchrotron radiation having a better resolution ($FWHM_{2\theta=90^\circ} \approx 0.1^\circ$) in comparison with the used classical diffractometer configuration ($FWHM_{2\theta=90^\circ} \approx 0.3^\circ$), the diffraction data showed the peak profiles more accurately. Consequently, the peak asymmetry was clearly seen when the peaks were fitted by symmetrical pseudo-Voigt function. The above-mentioned problems can be solved applying inverse analysis i.e. by recalculating the stress distribution $\sigma^I_{11}(\tau)$ from the determined $\sigma^I_{11}(z)$ and comparing the results with the experimental function.

To begin with, the first issue - the sensitivity of the stress at different depths z on the measured function $\sigma^I_{11}(\tau)$ - was studied. For this purpose the mean stress $\sigma^I_{11}(\tau)$ was computed using the equation:

$$\sigma^I_{ij}(\tau) = \int_0^x \sigma^I_{ij}(z) e^{-z/\tau} dz \Big/ \int_0^x e^{-z/\tau} dz \qquad (6)$$

where the integral was calculated up to different limits x and $\sigma^I_{11}(z)$ is the dependence of stress vs. real depth (z), shown in Figs. 7b and 8.

In Fig. 8 the continues lines represents the $\sigma^I_{ij}(\tau)$ dependence fitted to the experimental results approximated by second (a) and third order polynomials (b). According to definition (Eqs. (1) and (2) for $t \rightarrow \infty$), these functions are equal to the weighted integral calculated from function $\sigma^I_{11}(z)$, up to infinity for a bulk sample (consequently also $x \rightarrow \infty$ in Eq. (6)). The results of Eq. (6) computed for different limits x are compared with the measured stress $\sigma^I_{11}(\tau)$ represented in Fig. 8 by points and fitted continuous line. It was found that the recalculated profiles do not change

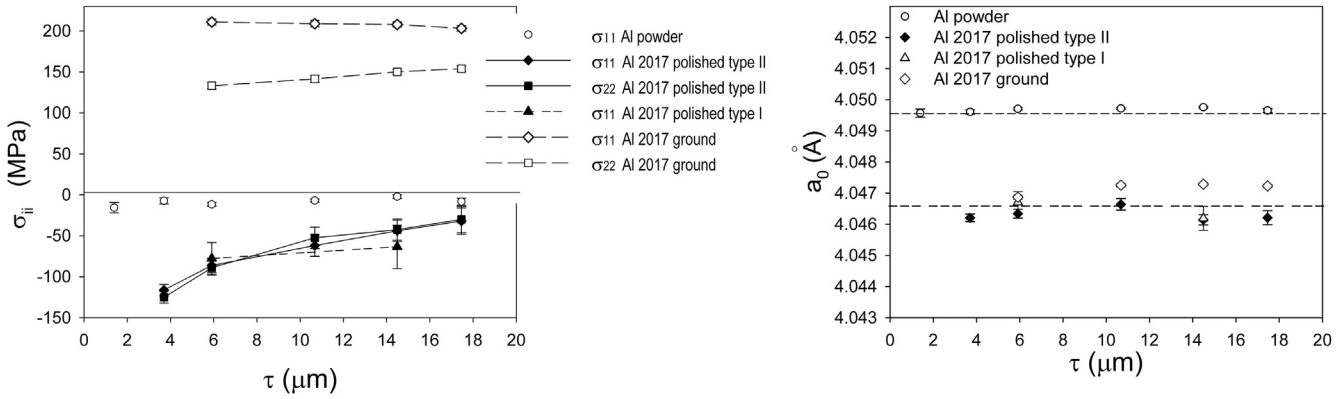

Fig. 4. The depth-dependent profiles of stress (σ^I_{11}) and a_0 parameter vs. penetration depth τ for mechanically polished (type I and II) and ground Al2017 samples, as well as the reference powder sample. The results obtained by MGIXD method with Cu K_α radiation are shown.

significantly and agree with the experiment if the integration is performed at least up to $x = 40$ μm, i.e. the stress over 40 μm does not significantly influence the measured values due to a low exponential weight in Eq. (6). Therefore, the $\sigma^I_{11}(z)$ dependence determined using the inverse Laplace method shows the real distribution of stress up to the approximate depth of 40 μm, while over this threshold the function $\sigma^I_{11}(z)$ has not physical meaning and the stress state is unknown. Finally, it should be also stated that it remains unproven that the obtained solution is unique.

For a deeper insight into the second mentioned problem, the experimental diffraction peak profiles were simulated. Each peak was modelled as the superposition of pseudo-Voigt functions having positions corresponding to the interplanar spacings modified by different stresses $\sigma^I_{11}(z)$ at different depths z. The XSF (Kröner method) were used in the calculation of lattice strains. The main problem of such modeling is that both FWHM and η parameter describing the contribution of the Lorentz component [16] are unknown and they can depend on the depth z. Only the dependence of peak intensity is known and described by absorption law. In this work the η parameter was assumed to be constant for different depths and it was determined by fitting pseudo-Voigt function to experimental peak for given *hkl* reflection (and corresponding 2θ). In the simulation, the superposed pseudo-Voigt profiles were weighted by intensity depending on absorption (corresponding to the depth z). Moreover, different dependences of FWHM on the depth were assumed in order to reproduce one of the most asymmetric peaks ($\lambda = 1.5419$ Å, $2\theta \approx 38.6°$ and $\alpha = 15°$). The following in-depth profile of FWHM $= b$ was assumed:

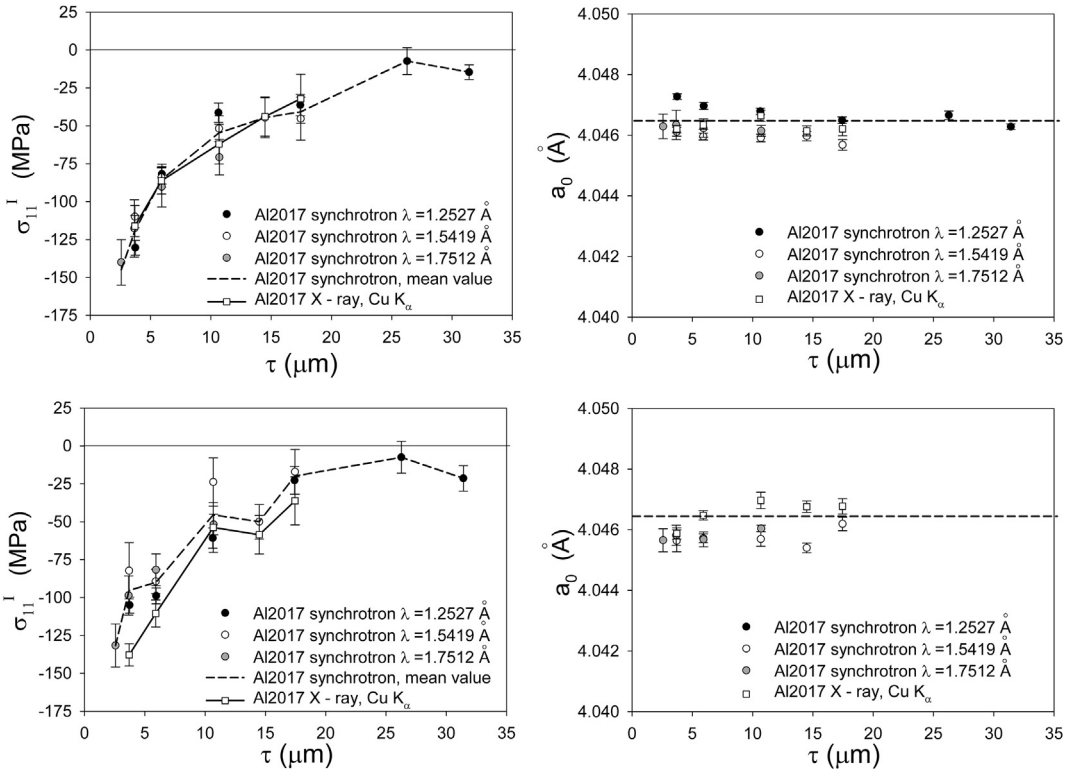

Fig. 5. The depth-dependent profiles of stress (σ^I_{11}) and a_0 lattice parameter vs. penetration depth τ for the polished (type II) sample. In the analysis the peak positions were determined by pseudo-Voigt function fitting (a) and using the centre of gravity method (b). The results for different wavelengths of synchrotron radiation and for Cu K_α radiation are compared.

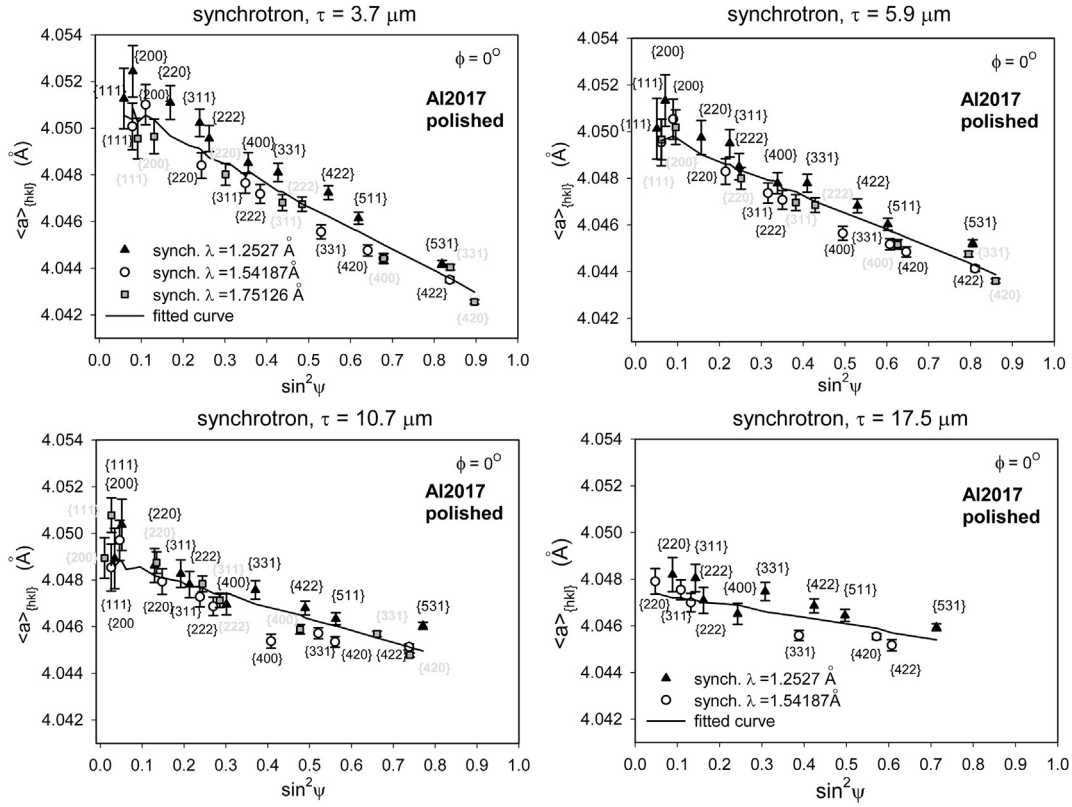

Fig. 6. The example of $\langle a.\phi,\psi)\rangle_{\{hkl\}}$ vs. $sin^2\psi$ plots for the polished (type II) sample obtained with three wavelengths (λ) and different incident angles (α). In each figure the experimental data corresponding to the same penetration depth are shown, together with the fitted theoretical line.

$$b = b_0 + b_1 \exp(-z/\xi) \tag{7}$$

where: b_0 is the FWHM for $z \to \infty$ and ξ, b_1 describes the evolution of FWHM for decreasing depth z, caused by microstructure variation due to polishing.

It was found that the experimental asymmetrical peak ($\lambda = 1.5419$ Å, $2\theta \approx 38.6°$ and $\alpha = 15°$) is correctly modelled for $\xi = 10$ μm and $b_0 = b_1$. In the calculations, the determined $\sigma^I_{11}(z)$ dependence was used and the model peak profiles were compared with the experimental points as well as with the calculations assuming zero stress (cf. Fig. 9a). In Fig. 9b, a similar comparison, but assuming constant FWHM, is shown. An important question is whether the other peaks (at different α, 2θ and for different λ) are also correctly reproduced for the FWHM evolution described by $\xi = 10$ μm. With this aim in mind, different peaks were modelled assuming the same variation of microstructure (corresponding to $\xi = 10$ μm in Eq. (7)) and the stress dependence $\sigma^I_{11}(z)$ shown in Fig. 7a. Only the values of b_0 (assuming $b_0 = b_1$) were adjusted individually for each diffraction peak (cf. Table 5). In Fig. 10 the experimental profiles were compared with the modelled ones assuming stress variation $\sigma^I_{11}(z)$ or stress equal to zero. The very good agreement between the experimental and theoretical peaks

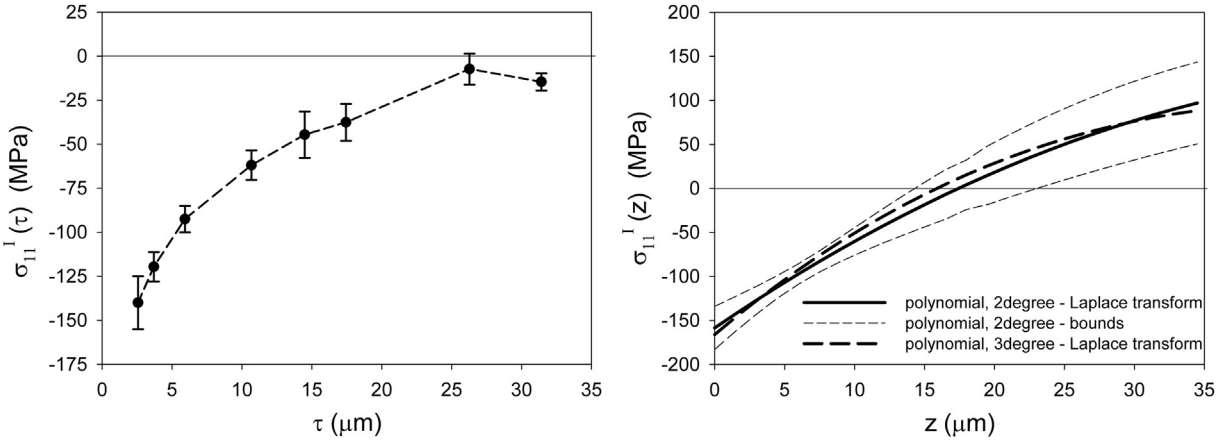

Fig. 7. The stress profile for the polished (type II) sample for all the experimental points obtained for the three different wavelengths as a function of τ - penetration depth (a) and z - real depth in sample (b). The uncertainty bounds are given for polynomial of 2nd degree.

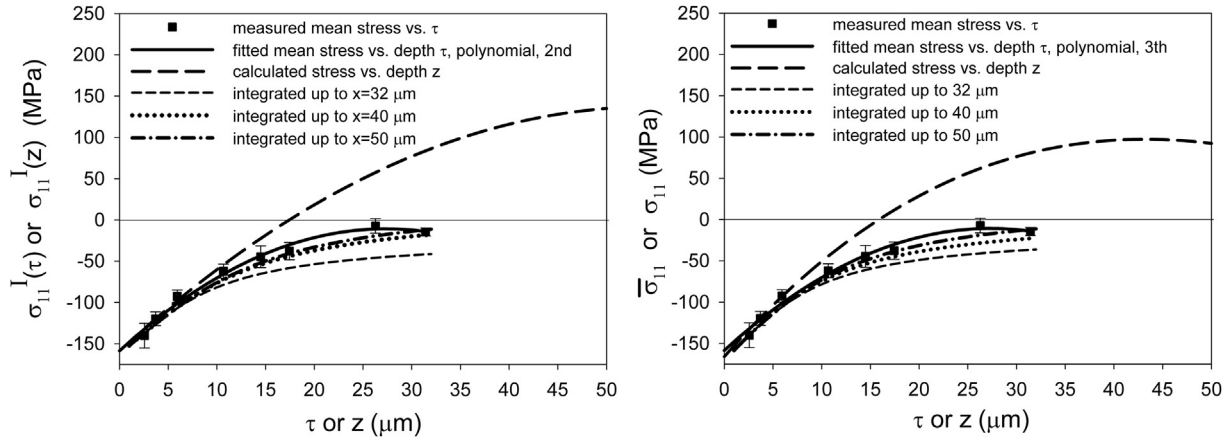

Fig. 8. The stress profiles for the polished (type II) sample: $\sigma^I_{11}(z)$ calculated from inverse Laplace transform, $\sigma^I_{11}(\tau)$ measured or recalculated from $\sigma^I_{11}(z)$ using Eq. (6). Polynomial of 2nd (a) and 3rd (b) degree were applied to fit the $\sigma^I_{11}(\tau)$ experimental values.

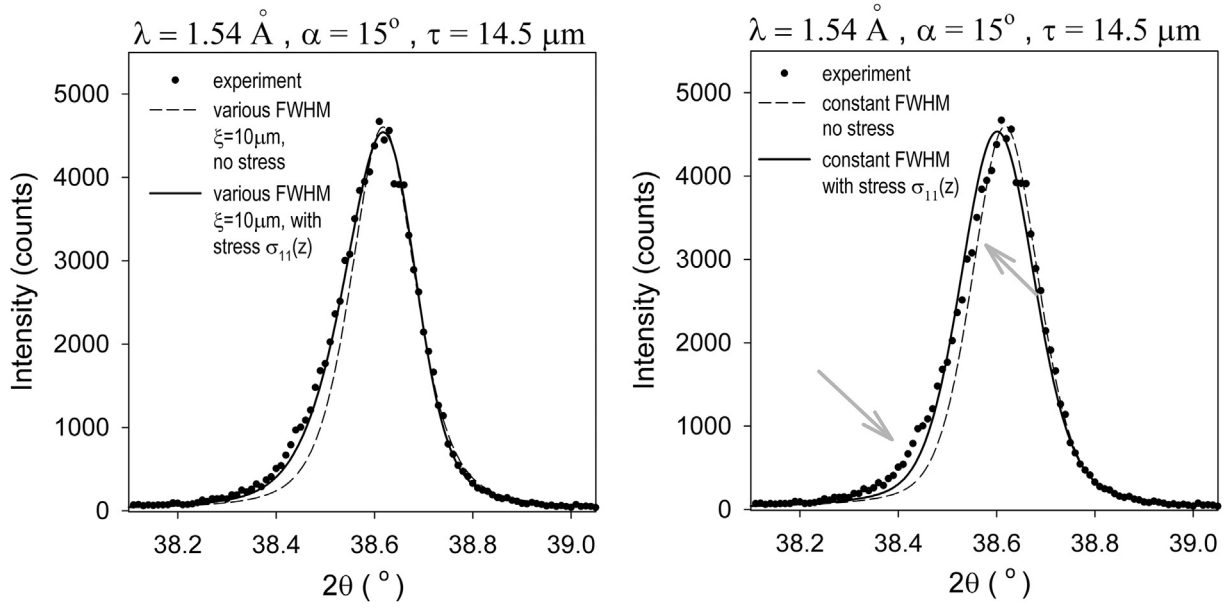

Fig. 9. A comparison of the diffraction peak profiles: experimental, simulated for $\sigma^I_{11}(z)$ stress function and assuming zero stress ($\lambda = 1.5419$ Å, $2\,\theta \approx 38.6°$ and $\alpha = 15°$). The results for FWHM variation described by Eq. (7) with $\xi = 10$ μm (a) and for constant FWHM (b) are shown.

confirms that the $\sigma^I_{11}(z)$ function correctly describes the stress depth-dependence. Moreover, it can also be seen that the stress gradient differently influences the diffraction peaks measured for different penetration depth. If the penetration depth τ is relatively small (in comparison with stress variation distance), compressive stress causes a significant shift of the diffraction peak ($\tau = 3.7$ μm, in Fig. 10), while for deeper penetration depth ($\tau = 14.5$ μm, in Fig. 10) the peak is not much shifted but significant asymmetry appears due to the superposition of the intensities from regions where compressive stress decreases and, next, changes to a tensile one.

It can be concluded that the inverse analysis (integration of stress $\sigma^I_{11}(z)$ with intensity weight) resulted in the determination of the maximum depth for which the stress influences diffraction results (about 40 μm). Consequently, for this depth the $\sigma^I_{11}(z)$ profile can be determined. Moreover, the inverse analysis applied for the peak profiles confirmed the stress distribution given by $\sigma^I_{11}(z)$. In the latter calculation, the increase of FWHM for the peak components coming from the regions closer to the surface was assumed. This effect is due to microstructure change caused by mechanical polishing (an increase of defects density and a decrease of crystallite size in the deformed material). It should be mentioned that a similar simulation of peak profile was also conducted by Genzel et al. [2] in order to explain the influence of stress gradient on the profile asymmetry. However, in that work the calculations were performed for one peak in the case of the deposited coating i.e. when constant FWHM can be assumed.

Table 5
Values of b_0 (assuming $b_0 = b_1$) used in modeling of the peaks for different $2\theta°$ angles and wavelengths.

	λ = 1.5419 Å			λ = 1.7512 Å			λ = 1.2527 Å		
2θ (°)	38.6	82.7	138.2	44.0	91.6	151.5	31.15	84.8	132.7
b_0 (°)	0.12	0.20	0.75	0.12	0.26	0.90	0.115	0.22	0.65

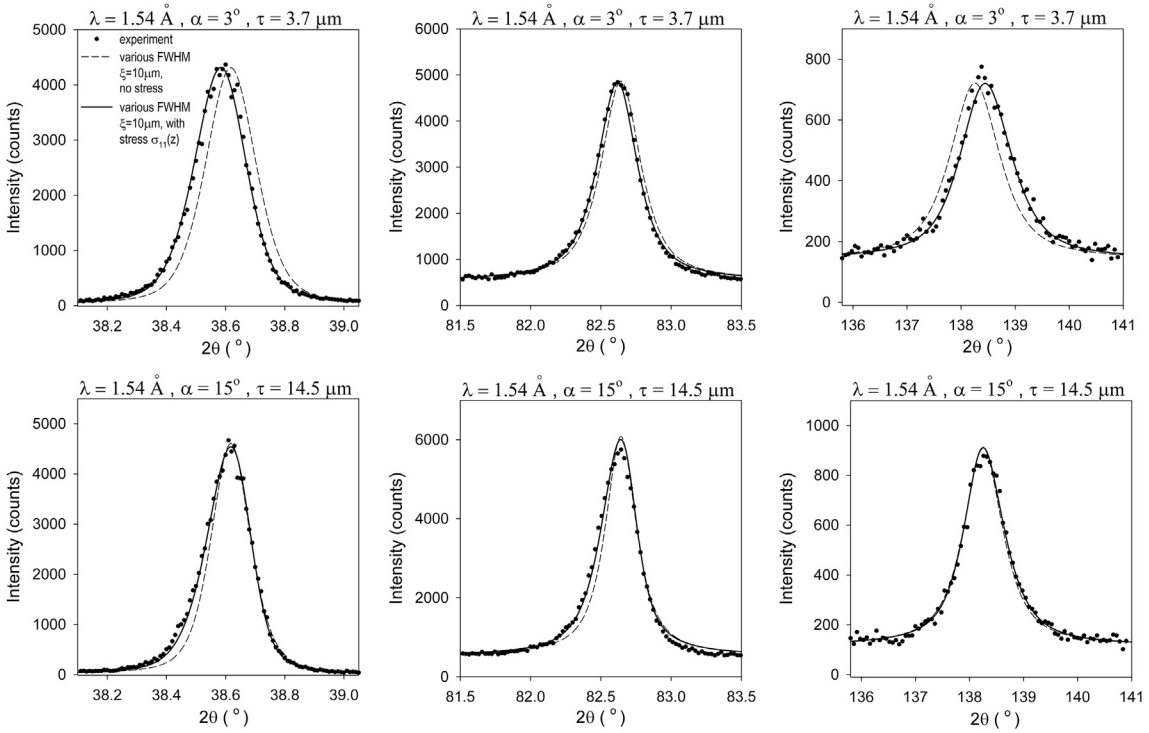

Fig. 10. A comparison of the diffraction peak profiles: experimental, simulated for $\sigma^{I}_{11}(z)$ stress function and assuming zero stress. For all the peaks (λ = 1.5419 Å), the same variation of FWHM described by Eq. (7) with ξ = 10 μm was used in the calculations ($b_0 = b_1$ is given in Table 5).

4. Summary

The MGIXD method was successfully verified and developed in order to increase the depth for which the stress gradient can be determined, therefore in the direction of more accurate residual stress determination. Not only different incident angles but also different wavelengths of X-ray radiation were used for this purpose. As a result, almost the same depth-dependent stress profiles were obtained for all the applied wavelengths, while the determined values of a_o did not vary significantly under the sample surface. Due to the very good resolution of the applied synchrotron radiation, it was possible to observe the diffraction peak asymmetry caused by the stress gradient, which was not possible to be investigated on the classical diffractometer. The stress depth-dependent distribution vs. real depth z was determined from the stress profile measured as the function of the information (or penetration) depth using the inverse Laplace transform. It should be stressed that it was not proven that the result of the Laplace transform is unique.

A deeper insight into the presented analysis, based on stress profile determined from inverse Laplace transform, resulted in the determination of the maximum depth for which the stress variation can be determined. Furthermore, the asymmetry of the obtained diffraction peaks measured by synchrotron radiation was explained by the determined stress gradient.

Acknowledgements

This work was financed by grants from the Polish National Scientific Centre (NCN): UMO-2014/15/D/ST8/00542 and DEC-2013/11/B/ST3/03787.

Furthermore, we would like to thank HASYLAB at DESY for the beamtime provided and Dr J. Donges for his assistance during the experiment at the G3 beamline.

References

[1] V. Hauk, Structural and Residual Stress Analysis by Nondestructive Methods, Elsevier, Amsterdam, 1997.
[2] Ch. Genzel, X-ray residual stress analysis in thin films under grazing incidence – basic aspects and applications, Mater. Sci. Technol. 21 (1) (2005) 10–18.
[3] M. Marciszko, A. Baczmański, K. Wierzbanowski, M. Wróbel, C. Braham, J.-P. Chopart, A. Lodini, T. Bonarski, L. Tarkowski, N. Zazi, Application of multi-reflection grazing incidence method for stress measurements in polished Al-Mg alloy and CrN coating, Appl. Surf. Sci. 266 (2013a) 256–267.
[4] M. Marciszko, A. Baczmański, M. Wróbel, W. Seiler, C. Braham, S. Wroński, R. Wawszczak, Problem of elastic anisotropy and stacking faults in stress analysis using multireflection grazing-incidence X-ray diffraction, J. Appl. Cryst. 48 (2015) 492–509.
[5] Ch. Genzel, Evaluation of stress gradients σij(z) from their discrete Laplace transforms σij(τk) obtained by x-ray diffraction performed in the scattered vector mode, Phys. Stat. Sol. (a) 156 (2) (1996) 353–363.
[6] H. Behnken, V. Hauk, Determination of steep stress gradients by X-ray diffraction results of joint investigation, Mater. Sci. Eng. A 300 (1–2) (2001) 41–51.
[7] T.C. Huan, P.K. Predecki, Grazing-incidence X-Ray Technique for Surface, Interface, and Thin-film Analysis, JCPDS-International Center for Diffraction Data, 1997.
[8] S.J. Skrzypek, A. Baczmański, W. Ratuszek, E. Kusior, New approach to stress analysis based on a grazing-incidence X-ray diffraction, J. Appl. Cryst. 34 (4) (2001) 427–435.
[9] U. Welzel, J. Ligot, P. Lamparter, A.C. Vermeulen, E.J. Mottemeijer, Stress analysis of polycrystalline thin film and surface regions by X-ray diffraction, J. Appl. Cryst. 38 (2005) 1–29.
[10] A. Baczmański, C. Braham, W. Seiler, N. Shiraki, Multi-reflection method and grazing incidence geometry used for stress measurement by X-ray diffraction, Surf. Coat. Technol. 182 (1) (2004) 43–54.
[11] M. Marciszko, A. Baczmański, M. Wróbel, W. Seiler, C. Braham, J. Donges, M. Śniechowski, K. Wierzbanowski, Multireflection grazing incidence diffraction used for stress measurements in surface layers, Thin Solid Films 530 (2013a) 81–84.
[12] S.J. Skrzypek, A. Baczmański, Progress in X-ray diffraction of residual macro-stress determination related to surface layer gradients and anisotropy, Adv.

X-ray Anal. 44 (2001) 134–145.
[13] G. Simoms, H. Wang, Single Crystal Elastic Constants and Calculated Aggregate Properties: a Handbook, second ed., The M.I.T. Press, Cambridge, Massachusetts and London, 1971.
[14] H.J. Bunge, Texture Analysis in Materials Science: Mathematical Methods, Butterworths and Co, London, 1982.
[15] A. Baczmański, C. Braham, W. Seiler, Microstresses in textured polycrystals studied by the multireflection diffraction method and self-consistent model, Philos. Mag. 83 (28) (2003) 3225–3246.
[16] W. Voigt, Lehrbuch der Kristallphysik, BG Teubner Verlag, Leipzig, 1928.